

# Self-Assembled Rigid Monolayers of 4'-Substituted-4-mercaptobiphenyls on Gold and Silver Surfaces

Jung F. Kang,<sup>†</sup> Abraham Ulman,<sup>\*,†</sup> Sheng Liao,<sup>†</sup> Rainer Jordan,<sup>†</sup>  
Guohua Yang,<sup>‡</sup> and Gang-yu Liu<sup>‡</sup>

Department of Chemical Engineering, Chemistry and Materials Science, and the NSF MRSEC for Polymers at Engineered Interfaces, Polytechnic University, Six Metrotech Center, Brooklyn, New York 11201, and Department of Chemistry, Wayne State University, Detroit, Michigan 48202

Received August 22, 2000

We have prepared, characterized, and studied self-assembled monolayers (SAMs) of rigid 4'-substituted-4-mercaptobiphenyls on planar Au(111) and Ag(111) substrates. These monolayers show lower contact angles than their corresponding alkanethiolate SAMs due to the polar nature of the aromatic moieties. Quantitative analysis of infrared spectroscopy, using Eulerian angle, allowed estimation of the average molecular orientation on a surface. In cases where such analysis is possible, it was found that the biphenyl planes are tilted away from the surface normal toward by 14°, 20°, and 12°, for NO<sub>2</sub>, C(O)CH<sub>3</sub>, and CO<sub>2</sub>Et, respectively, and rotate around the 1,4 axis of the ring at 30°, 15°, and 30° on gold, respectively. For SAMs on silver, the tilt is 8°, 21°, and 11°, respectively, and the rotation angle is 32°, 10°, and 31°, respectively, with errors  $\leq \pm 2^\circ$ . Scanning tunneling microscopy studies indicate that these plate-shaped molecules form incommensurate structures on Au(111) surfaces.

## Introduction

During the past 15 years, great progress has been made in the preparation of self-assembled monolayers (SAMs).<sup>1</sup> In contrast to ultrathin films made by, for example, molecular beam epitaxy (MBE)<sup>2</sup> or chemical vapor deposition (CVD), SAMs are highly ordered and oriented and can incorporate a wide range of groups both in the alkyl chain and at the chain terminus. Therefore, a variety of surfaces with specific interactions can be produced with fine structural control.<sup>3</sup> Due to their dense and stable structure, SAMs have potential applications in corrosion prevention<sup>4</sup> and lubrication.<sup>5</sup> In addition, these thin films have been important in studies of electron transfer,<sup>6</sup> molecular recognition,<sup>7</sup> biomaterial interfaces,<sup>8</sup> cell growth,<sup>9</sup> crystallization,<sup>10</sup> and many other systems.<sup>1,11</sup> Recently, SAMs have been utilized for nanopatterning using

microcontact ( $\mu\text{C}$ ) printing,<sup>12</sup> providing an exciting alternative to lithography in some applications.

Our interest in SAMs is as model surfaces for the studies of wetting,<sup>3</sup> adhesion,<sup>13</sup> and friction, and as starting materials for surface-initiated ionic polymerization.<sup>14</sup> Since surface properties are dominated by the outmost 5–10 Å of the organic material,<sup>15</sup> SAMs provide ideal model systems, due to the possible fine control of surface functional group concentration. These surfaces can be produced to have surface energies that span the range from "Teflon-like" surfaces (surface CF<sub>3</sub> groups) to very high-energy surfaces (surface OH or COOH groups), e.g., surface tensions of 10–70 dyn cm<sup>-1</sup>. For example, when the acidic protons in highly hydrophilic surfaces, e.g., OH, CONH<sub>2</sub>, and CO<sub>2</sub>H surfaces,<sup>16</sup> are substituted by methyl groups,<sup>17</sup> the surfaces become more hydrophobic, thus

\* To whom correspondence may be addressed. Phone: (718) 260-3119. Fax: (718) 260-3125. E-Fax: (810) 277-6217. E-mail: aulman@duke.poly.edu.

<sup>†</sup> Polytechnic University. Present address: Lehrstuhl für Makromolekulare Stoffe, Lichtenbergstr. 4, TU München, 85747 Garching, Germany.

<sup>‡</sup> Wayne State University.

(1) (a) Ulman, A. *An Introduction to Ultrathin Organic Films*; Academic Press: Boston, MA, 1991. (b) Ulman, A. *Chem. Rev.* **1996**, *96*, 1533.

(2) Forrest, S. R. *Chem. Rev.* **1997**, *97*, 1793.

(3) (a) Ulman, A.; Evans, S. D.; Shnidman, Y.; Sharma, R.; Eilers, J. E.; Chang, J. C. *J. Am. Chem. Soc.* **1991**, *113*, 1499.

(4) Laibinis, P. E.; Whitesides, G. M. *J. Am. Chem. Soc.* **1992**, *114*, 9022.

(5) Berman, A.; Steinberg, S.; Campbell, S.; Ulman, A.; Israelachvili, J. *Tribol. Lett.* **1998**, *43*.

(6) (a) Chidsey, C. E. D. *Science* **1991**, *251*, 919. Finklea, H. O.; Hanshaw, D. D. *J. Am. Chem. Soc.* **1992**, *114*, 3173. (b) Rowe, G. K.; Creager, S. E. *Langmuir* **1991**, *7*, 2307.

(7) (a) Mrksich, M.; Grunwell, J. R.; Whitesides, G. M. *J. Am. Chem. Soc.* **1995**, *117*, 12009. (b) Motesharei, K. Myles, D. C. *J. Am. Chem. Soc.* **1994**, *116*, 7413. (c) Spinke, J.; Liley, M.; Guder, H.-J.; Angermaier, L.; Knoll, W. *Langmuir* **1993**, *9*, 1821.

(8) (a) Mrksich, M.; Whitesides, G. M. *Annu. Rev. Biophys. Biomol. Struct.* **1996**, *25*, 55. (b) Yousaf, M. N.; Mrksich, M. *J. Am. Chem. Soc.* **1999**, *121*, 4286.

(9) (a) Tidwell, C. D.; Ertel, S. I.; Ratner, B. D.; Tarasevich, B. J.; Atre, S.; Allara, D. L. *Langmuir* **1997**, *13*, 3404. (b) Chen, C. S.; Mrksich, M.; Huang, S.; Whitesides, G. M.; Ingber, D. E. *Biotech. Prog.* **1998**, *14*, 356. (c) Houseman, B. T.; Mrksich, M. *J. Org. Chem.* **1998**, *63*, 7552.

(10) Zaccaro, J.; Kang, J. F.; Ulman, A.; Myerson, A. *Langmuir* **2000**, *16*, 3791.

(11) Bishop, A. R.; Nuzzo, R. G. *Curr. Opin. Colloid Interface Sci.* **1996**, *1*, 127.

(12) (a) Kumar, A.; Biebeck, H. A.; Abbott, N. L.; Whitesides, G. M. *J. Am. Chem. Soc.* **1992**, *114*, 9188. (b) Kumar, A.; Whitesides, G. M. *Appl. Phys. Lett.* **1993**, *63*, 2002. (c) Kumar, A.; Biebeck, H. A.; Whitesides, G. M. *Langmuir* **1994**, *10*, 1499. (d) Xia, Y.; Zhao, X.; Whitesides, G. M. *Microelectron Eng.* **1996**, *32*, 255. (e) Ross, C. B.; Sun, L.; Crooks, R. M. *Langmuir* **1993**, *9*, 632. (f) Jeon, N. L.; Nuzzo, R. G.; Xia, Y.; Mrksich, M.; Whitesides, G. M. *Langmuir* **1995**, *11*, 3024. (g) Xia, Y.; Mrksich, M.; Kim, E.; Whitesides, G. M. *J. Am. Chem. Soc.* **1995**, *117*, 9576. (h) Jeon, N. L.; Finnie, K.; Branshaw, K.; Nuzzo, R. G. *Langmuir* **1997**, *13*, 3382.

(13) Kim, S.; Choi, G. Y.; Ulman, A.; Fleischer, C. *Langmuir* **1997**, *13*, 6650.

(14) (a) Jordan, R.; Ulman, A., *J. Am. Chem. Soc.* **1998**, *120*, 243. (b) Jordan, R.; Ulman, A.; Kang, J. F.; Rafailovich, M.; Sokolov, J. *J. Am. Chem. Soc.* **1999**, *121*, 1016.

(15) Allara, D. L. In *Polymer Surfaces and Interfaces*; Feast, W. J., Munro, H. S., Richards, R. W., Eds.; Wiley: Chichester, 1993; Vol. II, p 27.

(16) Bain, C. D.; Troughton, E. B.; Tao, Y.-T.; Evall, J.; Whitesides, G. M.; Nuzzo, R. G. *J. Am. Chem. Soc.* **1989**, *111*, 321.

showing the sensitivity of wetting to the SAM surface functionality.

For the study of surface properties, SAMs must fulfill at least three requirements: (1) to be strongly attached to the substrate, and therefore be chemically and thermally stable; (2) to be homogeneous and close packed; and (3) to allow a diverse range of surface functional groups to be present. Alkanethiols readily give homogeneous, ordered, and chemically and mechanically stable SAMs<sup>1</sup> and hence provide excellent model systems.

The shortcoming of SAMs made of flexible alkyl derivatives, however, is that thermal disorder results in surface-*gauche* defects and thus surface disorder. Studies of sum-frequency vibration spectroscopy show that the structure of a surface is clearly perturbed when it interacts strongly with another condensed phase,<sup>18</sup> alerting us that structural perturbations need to be considered. This is especially serious for very polar surface groups, such as OH,<sup>19</sup> where the introduced disorder may be significant<sup>20</sup> and not confined to the surface.<sup>19</sup> Thus, one cannot preclude surface reorganization during adhesion experiments, for example, when poly(dimethylsiloxane) (PDMS) cross-linked networks interact with flexible SAM surfaces.<sup>21</sup>

Support for this suggestion may be found in a study of Siepmann and McDonald.<sup>22</sup> They carried out Monte Carlo simulations of CH<sub>3</sub>-terminated SAMs that are under the influence of compressive stress and found that the monolayers relax almost elastically after the stress is removed. Their observation was that under pressure surface *gauche* defects developed in 40% of the chains. These defects result in the exposure of CH<sub>2</sub> groups at the surface, which, for  $\omega$ -substituted alkyl chains with polar groups, results in a significant decrease in surface free energy. In the case where surface H-bonding interactions are enhanced due to surface reorganization, the latter may not be reversible.<sup>19</sup> Therefore, a preferred system will be one in which conformational disorder has been eliminated, as completely as possible. This can be achieved by using rigid molecules, where surface functional groups have no conformational freedom and are "stuck" at the surface.

Bard and co-workers described SAMs made of rigid thiols;<sup>23</sup> however, these molecules exhibit a large cross-sectional area that results in a sizable mismatch with the size of many substituents. Therefore, we searched for rigid molecules that will spontaneously give layered structures. It was postulated that if the bulk crystal of a molecule can be viewed as a commensurate assembly of two-dimensional layers,<sup>24</sup> this molecule might be an excellent candidate for SAM formation. Studies of 4,4'-dioctylbiphenyl, which spontaneously forms stable suspended liquid crystal (SLC) films,<sup>25</sup> were carried out. The results suggest that 4'-substituted-4-mercapto-biphenyl derivatives (Figure 1)

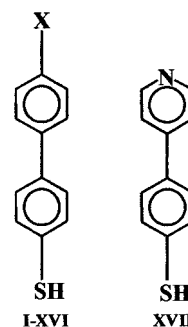


**Figure 1.** 4-Mercaptobiphenyls.

may form ordered SAMs on Au(111) surfaces.<sup>26</sup> Beyond their rigidity, the advantage of these aromatic thiols is the conjugation between the adsorbing thiolate and the 4'-substituent. This conjugation affects the acidity of the thiol proton and, hence, may make the thiolate a softer or a harder ligand.<sup>27</sup> Since the thiolate is an electron-donating group, an electron-attracting substituent will result in a significant molecular dipole moment. Dipolar interactions may alter adsorption kinetics<sup>28</sup> and the composition of mixed SAMs in equilibrium,<sup>29</sup> as became apparent from recent studies in our group.

Independently, Rubinstein and co-workers assembled thiophenol, 4-mercaptobiphenyl, and 4-mercaptoterphenyl onto gold and reported that the latter two formed reproducible SAMs that were substantially more stable than those from mercaptophenol, presumably due to greater intermolecular  $\pi$ - $\pi$  interactions.<sup>30</sup> Using molecular mechanics calculations, they predicted a herringbone structure for the adsorbed 4-mercaptoterphenyl with molecules oriented close to the surface normal. Recent molecular dynamics simulations in our group confirmed this structure and suggested tilt angles of  $\leq 15^\circ$ .<sup>31</sup>

Sita and co-workers have examined a related set of compounds where acetylenic units were located between the phenyl rings.<sup>32</sup> Using scanning tunneling microscopy (STM), they reported the formation of ordered domains for the species on gold. Tour and co-workers have synthesized an expanded collection of phenyl, biphenyl, and terphenyl derivatives, both with and without acetylenic units that link the phenyl rings, and characterized SAMs derived from them.<sup>33</sup> They suggested using rigid, conjugated molecules as molecular conductors, and Chidsey and co-workers measured the rates of interfacial electron transfer<sup>34</sup> through similar systems prepared by Sita and co-workers.<sup>35</sup> Finally, Tao and co-workers applied cyclic voltammetry (CV) to study the structure of aromatic-derivatized thiol monolayer on gold.<sup>36</sup> They showed that

(17) Laibinis, P. E.; Whitesides, G. M. *J. Am. Chem. Soc.* **1992**, *114*, 1990.

(18) Ong, T. H.; Ward, R. N.; Davies, P. B.; Bain, C. D. *J. Am. Chem. Soc.* **1992**, *114*, 6243.

(19) Evans, S. D.; Sharma, R.; Ulman, A. *Langmuir* **1991**, *7*, 156.

(20) (a) Kacker, N.; Kuman, S. K.; Allara, D. L. *Langmuir* **1997**, *13*, 6366. (b) Hautman, J.; Klein, M. L. *Phys. Rev. Lett.* **1991**, *67*, 1763. (c) Hautman, J.; Bareman, J. P.; Mar, W.; Klein, M. L. *J. Chem. Soc., Faraday Trans.* **1991**, *87*, 2031.

(21) Chaudhury, M. K.; Whitesides, G. M. *Langmuir* **1991**, *7*, 1013.

(22) Siepmann, J. I.; McDonald, I. R. *Phys. Rev. Lett.* **1993**, *70*, 453.

(23) (a) Kim, Y.-T.; McCarley, R. L.; Bard, A. J. *J. Phys. Chem.* **1992**, *96*, 7416. (b) Obeng, Y. S.; Laing, M. E.; Friedli, A. C.; Yang, H. C.; Wang, D.; Thulstrup, E. W.; Bard, A. J.; Michl, J. *J. Am. Chem. Soc.* **1992**, *114*, 9943.

(24) Scaringe, R. P. In *Electron Crystallography of Organic Molecules*; Fryer, J. R., Dorset, D. L., Eds.; Kluwer: Dordrecht, 1990; pp 85–113.

(25) Young, C. Y.; Pindak, R.; Clark, N. A.; Meyer, R. B. *Phys. Rev. Lett.* **1978**, *40*, 773.

(26) Ulman, A.; Scaringe, R. *Langmuir* **1992**, *8*, 894.

(27) (a) Pearson, R. G.; Songstand, J. *J. Am. Chem. Soc.* **1967**, *89*, 1827. (b) Pearson, R. G. *J. Chem. Educ.* **1968**, *45*, 581, 643.

(28) Liao, S.; Ulman, A.; Shnidman, Y. *J. Am. Chem. Soc.*,

(29) (a) Kang, J. F.; Liao, S.; Jordan, R.; Ulman, A. *J. Am. Chem. Soc.* **1998**, *120*, 9662. (b) Kang, J. F.; Ulman, A.; Liao, S.; Jordan, R. *Langmuir* **1999**, *15*, 2095.

(30) Sabatani, E.; Cohen-Boulakia, J.; Bruening, M.; Rubinstein, I. *Langmuir* **1993**, *9*, 2974.

(31) Wong, J.; Shnidman, Y.; Ulman, A. Unpublished results.

(32) (a) Dhirani, A.-A.; Zehner, R. W.; Hsung, R. P.; Guyot-Sionnest, P.; Sita, L. R. *J. Am. Chem. Soc.* **1996**, *118*, 3319–3320. (b) Zehner, R. W.; Sita, L. R. *Langmuir* **1997**, *13*, 2973. (c) Zehner, R. W.; Pearson, B. F.; Hsung, R. P.; Sita, L. R. *Langmuir* **1999**, *15*, 1121.

(33) (a) Tour, J. M.; Jones, L., II; Pearson, D. L.; Lamba, J. J. S.; Burgin, T. P.; Whitesides, G. M.; Allara, D. L.; Parikh, A. N.; Atre, S. *J. Am. Chem. Soc.* **1995**, *117*, 9529. (b) Jones, L., II; Schumm, J. S.; Tour, J. M. *J. Org. Chem.* **1997**, *62*, 1388. (c) Pearson, D. L.; Tour, J. M. *J. Org. Chem.* **1997**, *62*, 1376.

(34) Sachs, S. B.; Dudek, S. P.; Chidsey, C. E. D. *J. Am. Chem. Soc.* **1997**, *119*, 10563.

for phenyl-substituted thiols, the stability of a monolayer formed on gold depended on the location of the benzene ring in the alkyl chain, as well as on the length of this chain.

There are several advantages to using the 4'-substituted-4-mercaptobiphenyl system (Figure 1). First is the fact that thiolate SAMs on Au(111) have been studied more than any other SAM, and many structural and physical properties are well understood.<sup>1,11</sup> A second advantage is the simple synthetic routes for the preparation of thiophenols,<sup>31</sup> non-moisture-sensitive solid compounds. Third is the potential epitaxial adsorption of the thiolate-add-layer on the gold lattice and, therefore, the possibility that using different underlying lattices may provide surfaces with different symmetries. Last is the ability to alter the adsorbing properties of the thiolate by using different substituents at the 4'-position of the biphenyl moiety. Structural differences between alkanethiolate adsorption on Au(111) and Ag(111) result from differences in the electronic structure of these metals.<sup>37</sup> Similarly, adsorption of different 4'-substituted-4-mercaptobiphenyls on Au(111) may result in different monolayer structures.

Mohri et al. reported that 4-aminobenzenethiol is spontaneously oxidized to 4,4'-diaminodiphenyl disulfide in the presence of gold powder.<sup>38</sup> This result hints that the stability of thiolate SAMs on gold may be related to the electron density on the thiolate sulfur. The series of 4-mercaptobiphenyls reported here would allow further studies to elucidate this question.

This paper describes the preparation and characterization of self-assembled SAMs formed by the chemisorption of 4'-substituted-4-mercaptobiphenyls (X-(C<sub>6</sub>H<sub>4</sub>)<sub>2</sub>-SH) on surfaces of gold and silver. A series of thiols was prepared (Figure 1) to provide a variety of chemical functionalities for surface modification and engineering. 4'-Substituted-4-mercaptobiphenyls were prepared where X in Figure 1 is CF<sub>3</sub> (I), CH<sub>3</sub> (II), SCH<sub>3</sub> (III), OH (IV), NO<sub>2</sub> (V), N(CH<sub>3</sub>)<sub>2</sub> (VI), F (VII), Cl (VIII), Br (IX), I (X), CO<sub>2</sub>Et (XI), CHOCH<sub>3</sub> (XII), OCH<sub>2</sub>CH<sub>2</sub>OMe (XIII), -SH (XIV), -C(O)CH<sub>3</sub> (XV), and H (XVI).

## Experimental Section

**Materials.** Commercial reagents were ACS grade or higher and were used without further purification. All solvents were obtained from Aldrich. Anhydrous ethanol was obtained from Quantum Chemicals. A typical procedure for the preparation of 4'-substituted-4-mercaptobiphenyls is described below.

**4'-Methoxy-4-mercaptobiphenyl** was prepared by palladium-assisted coupling of 4-methylthiophenylmagnesium bromide and 4-iodoanisole. Thus, the Pd(PPh<sub>3</sub>)<sub>4</sub> catalyst (0.2 mmol, Aldrich) was added to 4.68 g (20 mmol) 4-iodoanisole (Aldrich) in 5 mL of absolute THF (Aldrich), and the solution was brought to gentle reflux under dry nitrogen. A Grignard solution, prepared in the usual way from 1-bromo-4-methylthiobenzene (4.06 g, 20 mmol, Aldrich) and magnesium (22 mg-atom, Kodak) in 25 mL of THF, was transferred to the boiling 4-iodoanisole solution using 1/8-in. Teflon tubing. The entire system was under nitrogen, and nitrogen pressure was used to control the addition rate. The reaction was exothermic. First, the solution became clear, and then magnesium salts started to deposit. After the addition was completed, the mixture was refluxed for an additional 30 min. After cooling, the reaction mixture was poured into ice water

(100 mL) containing 5 mL of HCl. The solid was filtered, washed with water, dried, and crystallized from heptane/2-propanol. The yield was 68%.

**4'-Hydroxy-4-mercaptobiphenyl.** 4-Methoxy-4'-methylthiobiphenyl (3.06 g, 20 mmol) was dissolved in 30 mL of dry DMF (Aldrich) under a nitrogen blanket. C<sub>2</sub>H<sub>5</sub>SK (4.6 g, 50 mmol) was added to the stirred solution, and it was refluxed gently for 6 h. After cooling, the solution was poured into ice water (100 mL) containing 5 mL of HCl. The solid was collected, washed with cold water, air-dried, and crystallized from heptane/2-propanol. The yield of 4'-hydroxy-4-mercaptobiphenyl was 78%. The structure of the product was confirmed by <sup>1</sup>H NMR spectroscopy.

**4'-Substituted-4-tert-butylthiobiphenyl.** In an alternative route a Grignard solution, prepared in the usual way from 1-bromo-4-tert-butylthiobenzene (6.44 g, 20 mmol) and magnesium (22 mg-atom, Kodak) in 25 mL of THF, was transferred to a boiling solution of 4-substitutedbenzene iodide and Pd(PPh<sub>3</sub>)<sub>4</sub> catalyst (0.2 mmol, Aldrich) in 5 mL of absolute THF (Aldrich) using a 1/8-in. Teflon tubing. The reaction was continued as above. The product was purified on a SiO<sub>2</sub> chromatographic column using a mixture of heptane/ethyl acetate. The ratio of the mixture depends on the 4'-substituent.

**4'-Substituted-4-mercaptobiphenyl.** A 10-mmol portion of 4'-substituted-4-tert-butylthiobiphenyl was dissolved in 25 mL of chloroform. An 11-mmol portion of Hg(ClO<sub>4</sub>)<sub>2</sub>X<sub>4</sub>H<sub>2</sub>O in 10 mL of methanol was added under stirring. A yellow precipitate appeared immediately. The reaction mixture was stirred for additional 30 min; thereafter H<sub>2</sub>S was bubbled and a black precipitate of HgS appeared. The mixture was filtered and the solid was washed with chloroform. The organic solution was washed with water (2 × 50 mL), 5% NaHCO<sub>3</sub> (50 mL), and water (50 mL) and dried over anhydrous Na<sub>2</sub>SO<sub>4</sub>. The chloroform was removed under reduced pressure and the product was crystallized from heptane/2-propanol or heptane/toluene.

**4'-Trifluoromethyl-4-mercaptobiphenyl (I):** mp 123 °C; <sup>1</sup>H NMR (δ ppm, CDCl<sub>3</sub>) 3.15 (s, 1H), 7.41 (AB, J = 8.37, Δν = 32.94 Hz, 4H), 7.65 (AB, J = 8.69, Δν = 12.29 Hz, 4H).

**4'-Methyl-4-mercaptobiphenyl (II):** mp 140 °C; <sup>1</sup>H NMR (δ ppm, J in Hz, CDCl<sub>3</sub>) 2.38 (s, 3H), 3.47 (s, 1H), 7.11 (AB, J = 8.69, Δν = 201.77 Hz, 4H), 7.36 (AB, J = 8.97, Δν = 46.49 Hz, 4H);

**4'-Methylthio-4-mercaptobiphenyl (III):** mp 149 °C; <sup>1</sup>H NMR (δ ppm, J in Hz, CDCl<sub>3</sub>) 2.50 (s, 3H), 3.47 (s, 1H), 7.31 (overlapped AB, 4H); 7.43 (AB, J = 8.41, Δν = 19.01 Hz, 4H).

**4'-Hydroxy-4-mercaptobiphenyl (IV):** mp 178 °C; <sup>1</sup>H NMR (δ ppm, J in Hz, DMF-*d*<sub>7</sub>) 3.42 (s, broad, 1H), 6.93 (d, J = 8.77, half AB, 2H), 7.40 (d, J = 8.43, half AB, 2H), 7.52 (m, 4H), 9.70 (s, broad, 1H).

**4'-Nitro-4-mercaptobiphenyl (V):** mp 162 °C; <sup>1</sup>H NMR (δ ppm, J in Hz, CDCl<sub>3</sub>) 2.38.

**4'-Dimethylamino-4-mercaptobiphenyl (VI):** mp 178 °C; <sup>1</sup>H NMR (δ ppm, J in Hz, CDCl<sub>3</sub>) 2.98 (s, 6H), 3.44 (s, 1H), 7.11 (AB, J = 8.69, Δν = 201.77 Hz, 4H), 7.36 (AB, J = 8.97, Δν = 46.49 Hz, 4H).

**4'-Fluoro-4-mercaptobiphenyl (VII):** mp 91 °C; <sup>1</sup>H NMR (δ ppm, J in Hz, CDCl<sub>3</sub>) 2.48 (s, 1H), 7.18 (m, 2H), 7.37 (AB, J = 8.56, Δν = 23.77 Hz, 4H), 7.50 (m, 2H).

**4'-Chloro-4-mercaptobiphenyl (VIII):** mp 152 °C; <sup>1</sup>H NMR (δ ppm, J in Hz, CDCl<sub>3</sub>) 2.49 (s, 1H), 7.40 (m, 8H).

**4'-Bromo-4-mercaptobiphenyl (IX):** mp 151 °C; <sup>1</sup>H NMR (δ ppm, J in Hz, CDCl<sub>3</sub>) 3.49 (s, 1H), 7.40 (AB, J = 8.59, Δν = 63.58 Hz, 4H), 7.42 (m, 4H).

**4'-Iodo-4-mercaptobiphenyl (X):** mp 175 °C; <sup>1</sup>H NMR (δ ppm, J in Hz, CDCl<sub>3</sub>) 3.48 (s, 1H), 7.34 (AB, J = 0.428, Δν = 141.70 Hz, 4H), 7.53 (AB, J = 8.38, Δν = 125.08 Hz, 4H).

**4'-Ethoxycarbonyl-4-mercaptobiphenyl (XI):** mp 75 °C; <sup>1</sup>H NMR (δ ppm, J in Hz, CDCl<sub>3</sub>) 1.40 (t, J = 7.18 Hz, 3H), 3.51 (s, 1H), 4.38 (q, J = 7.18, 2H), 7.41 (AB, J = 8.25, Δν = 43.15 Hz, 4H), 7.84 (AB, J = 8.35, Δν = 145.28 Hz, 4H).

**4'-(1-Hydroxyethyl)-4-mercaptobiphenyl (XII):** mp 254 °C; <sup>1</sup>H NMR (δ ppm, J in Hz, CDCl<sub>3</sub>) 1.52 (d, J = 6.45, 3H), 1.69 (s, broad, 1H), 3.48 (s, 1H), 4.94 (q, J = 6.45, 1H), 7.43 (AB, J = 8.22, Δν = 61.18 Hz, 4H), 7.44 (overlapped AB, 4H).

**4'-(Methoxyethoxy)-4-mercaptobiphenyl (XIII):** mp 128 °C; <sup>1</sup>H NMR (δ ppm, J in Hz, CDCl<sub>3</sub>) 3.35 (s, 3H), 3.58 (s, 1H),

(35) (a) Hsung, R. P.; Babcock, J. R.; Chidsey, C. E. D.; Sita, L. R. *Tetrahedron Lett.* **1995**, *36*, 4525. (b) Hsung, R.; Chidsey, C. E. D.; Sita, L. R. *Organometallics* **1995**, *14*, 4808.

(36) Tao, Y. T.; Wu, C. C.; Eu, J. Y.; Lin, W. L. *Langmuir* **1997**, *13*, 4018.

(37) Sellers, H.; Ulman, A.; Shnidman, Y.; Eilers, J. E. *J. Am. Chem. Soc.* **1993**, *115*, 9389.

(38) Mohri, N.; Inoue, M.; Arai, Y.; Yoshikawa, K. *Langmuir* **1995**, *11*, 1612.

3.67 (t, equal heights, 2H), 4.10 (t, equal heights, 2H), 6.95 (m, 2H), 7.42 (m, 1H), 7.76 (m, 5H).

**4,4'-Dimercaptobiphenyl (XIV):** mp 180 °C; <sup>1</sup>H NMR ( $\delta$  ppm, J in Hz, CDCl<sub>3</sub>) 3.48 (s, 2H), 7.38 (AB,  $J = 5.30$ ,  $\Delta\nu = 29.60$  Hz, 8H).

**4'-Acetyl-4-mercaptobiphenyl (XV):** mp 114 °C; <sup>1</sup>H NMR ( $\delta$  ppm, J in Hz, CDCl<sub>3</sub>) 2.62 (s, 3H), 3.52 (s, 1H), 7.37 (AB,  $J = 5.68$ ,  $\Delta\nu = 43.39$  Hz, 4H), 7.81 (AB,  $J = 8.32$ ,  $\Delta\nu = 112.81$  Hz, 8H).

**4-Mercaptobiphenyl (XVI):** mp 102 °C; <sup>1</sup>H NMR ( $\delta$  ppm, J in Hz, CDCl<sub>3</sub>) 3.48 (s, 1H), 7.44 (m, 9H).

**4-(4-Mercaptophenyl)pyridine (XVII):** mp 103 °C; <sup>1</sup>H NMR ( $\delta$  ppm, J in Hz, CDCl<sub>3</sub>) 3.54 (s, 1H), 7.43 (AB,  $J = 8.32$ ,  $\Delta\nu = 43.82$  Hz, 4H), 8.04 (AB,  $J = 6.18$ ,  $\Delta\nu = 354.86$  Hz, 4H).

**Gold and Silver Substrate Preparation.** Details of gold substrate preparation were published before.<sup>14,29,39</sup> In short, glass slides were baked overnight in vacuum ( $\leq 10^{-6}$  Torr) at 300 °C. Gold (99.99%) evaporation was carried out at the same temperature, using a constant deposition rate of 3 Å/s. The gold thickness was 1000 Å. The gold substrates were further annealed in vacuum at 300 °C for 18 h. Reproducible optical constants for gold substrates prepared according to this procedure are  $N_s = 0.186 \pm 0.01$  and  $K_s = 3.400 \pm 0.05$ . Except for an annealing temperature at 150 °C and deposited film thickness at 1500 Å the procedure for preparing silver film is the same as that for preparing gold film. Reproducible optical constants for silver substrates prepared in this manner are  $N_s = 0.054 \pm 0.01$ , and  $K_s = 4.278 \pm 0.1$ . The optical constants for gold and silver surfaces were measured at  $\lambda = 632.8$  nm and are in agreement with the classical data of Johnson and Crispy.<sup>40</sup>

**Monolayer Preparation.** Gold substrates were cleaned by argon plasma for 30 s, directly before being immersed into the thiol solution (10  $\mu$ M) in ethanol, under nitrogen, and kept there overnight. The substrates were removed from solution, rinsed with ethanol, and blown dry by a jet of nitrogen. Silver substrates were cleaned by argon plasma for 10 s before immersion in the thiol solution (1  $\mu$ M) in ethanol. Silver substrates showed significant tendency to induce multilayer formation, much more than gold.

**Thickness Measurements.** Thickness was estimated by ellipsometry using a Rudolph Research AutoEL ellipsometer (He-Ne laser,  $\lambda = 632.8$  nm, angle of incidence 70°). Three separate points were measured on each sample, using an assumed refractive index of 1.462 for the SAM. The variation of measured thickness for biphenyl thiol monolayer was  $\pm 1-2$  Å.

**Contact Angle Measurements.** Contact angle were determined by the sessile drop method using a Rame-Hart model 100 goniometer, equipped with a high-resolution CCD-IRIS color video-camera (Sony) connected to a computer, at room temperature. To measure the advancing and receding angles, a 20- $\mu$ L droplet was formed at the end of blunt-ended needle of a syringe, whose position is controlled and fixed for each measurement. The image of the droplet has been observed on the computer monitor and saved as a picture file. Advancing and receding angles were measured by tilting the sample stage. Thus, the tilt angle was increased until the droplet started to move on the surface and immediately decreased to a point where the droplet stopped moving. All contact angles reported here are the average of 25 readings made on five independently prepared SAMs. The accuracy of measurements is  $\pm 1^\circ$ .

**External Reflection Fourier Transform Infrared Spectroscopy (FTIR).** The IR data were obtained using a Nicolet MAGNA-IR 760 spectrometer equipped with an MCT-A detector cooled with liquid nitrogen. The sample compartment was purged with CO<sub>2</sub>-free dry air. Spectra were collected in a grazing angle mode using a Spectratech FT-80 attachment (angle of incidence 80°). A total of 2500 scans were collected for each spectrum, with resolution of 1 cm<sup>-1</sup>. The deviation of band position is  $\pm 0.3$  cm<sup>-1</sup>.

**X-ray Diffraction.** The structure of evaporated gold and silver films was studied using a XRG 3100 X-ray generator with Cu K $\alpha$  radiation ( $\lambda = 1.5418$  Å). The values  $a_0 = 4.070$  and 4.077 Å were obtained for the polycrystalline gold and silver surfaces in face-center cubic (fcc) structure, respectively.

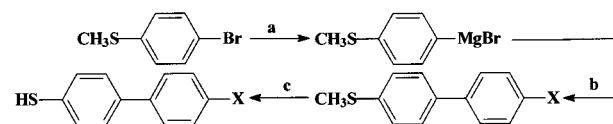


**Figure 2.** Synthesis of 4'-substituted-4-mercaptobiphenyls: (a) Mg/THF/N<sub>2</sub>; (b) X-C<sub>6</sub>H<sub>4</sub>-I(Br)/[(Ph<sub>3</sub>P)<sub>4</sub>Pd]/THF/D/N<sub>2</sub>; (c) C<sub>2</sub>H<sub>5</sub>S<sup>-</sup>K<sup>+</sup>/DMF.

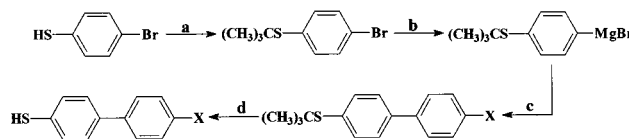


**Figure 3.** Synthesis of 4'-substituted-4-mercaptobiphenyls: (a) (CH<sub>3</sub>)<sub>2</sub>C=CH<sub>2</sub>/H<sup>+</sup>; (b) Mg/THF/N<sub>2</sub>; (c) X-C<sub>6</sub>H<sub>4</sub>-I(Br)/[(Ph<sub>3</sub>P)<sub>4</sub>Pd]/THF/D/N<sub>2</sub>; (d) Hg(ClO<sub>4</sub>)<sub>2</sub>/CHCl<sub>3</sub>/CH<sub>3</sub>OH.

**Scanning Probe Microscopy Techniques.** Atomic force microscopy (AFM) of the gold and silver substrates was performed with a Nanoscope III (digital instruments) in contact mode. Monolayers of 4'-chloro-4-mercaptobiphenyls were prepared by soaking freshly prepared Au(111) films into a 0.02 mM dichloromethane or ethanol solution for 18–72 h under a nitrogen atmosphere. After a thorough cleaning by dichloromethane and ethanol, the samples were immediately transferred into ultrahigh vacuum (UHV) for STM study. The STM scanner has a walker type configuration (RHK Technology, Inc.) and is operated under UHV conditions ( $3 \times 10^{-10}$  Torr). The STM tips are 0.25 mm tungsten wires electrochemically etched in 3 M KOH. All STM images were acquired in high-impedance, constant current mode. The tunneling current was set between 10 and 200 pA, and the bias voltage was varied between -2.0 and 2.0 V.

## Results and Discussion

Mercaptobiphenyl derivatives were prepared using a palladium coupling reaction.<sup>41</sup> Two main routes were employed. In the first (Figure 2), methylthiophenylmagnesium bromide was coupled with 4-substituted iodobenzenes, and the methyl protecting-group was removed using potassium ethanethiolate in DMF.

In the second (Figure 3) the thiophenol group was converted to the corresponding *tert*-butylthioether by reacting 4-bromomercaptophenol with isobutylene in dichloromethane in the presence of an acidic ion-exchange resin. The *tert*-butyl thioether was converted to the corresponding magnesium bromide derivative in THF, and the latter was added to a boiling solution of the 4-substituted iodo(bromo)benzene in THF, under nitrogen, with [(Ph<sub>3</sub>P)<sub>4</sub>Pd] as the catalyst. After reaction was complete, the protecting group was removed by treating the chloroform solution of the thioether with Hg(ClO<sub>4</sub>)<sub>2</sub> in methanol, followed by bubbling H<sub>2</sub>S. All thiols were purified by chromatography on silica gel and crystallized twice.

The gold and silver films (1000 and 1500 Å in thickness, respectively) were deposited on glass slides by vapor deposition. To enable annealing of gold substrates, the adhesion layer of chromium (or titanium) was eliminated. This became possible when the glass slides were baked overnight in vacuum ( $\leq 10^{-6}$  Torr) at 300 °C. The process results in an apparent complete removal of organic contaminants and of adsorbed water. Furthermore, at this temperature surface silanol groups form siloxane groups, thus reducing surface hydrophilicity and acidity. As a result, adhesion of gold is improved significantly and no peeling off could be detected during the immersion in the thiol solution.

(39) Kang, J. F.; Jordan, R.; Ulman, A. *Langmuir* **1998**, *14*, 3983.  
(40) Johnson, C. *Phys. Rev. B* **1972**, *6*, 4370.

(41) Heck, R. F. *Palladium Reagents in Organic Synthesis*; Academic Press: London, 1985.

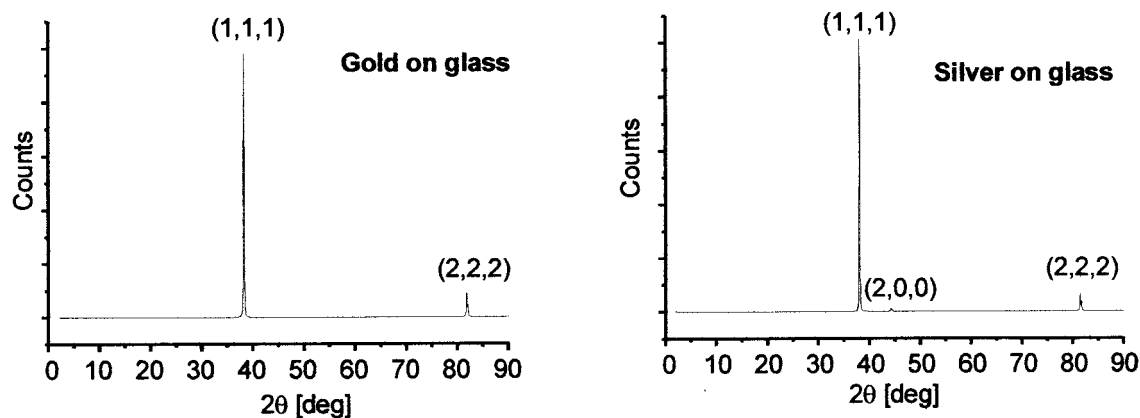


**Figure 4.** X-ray diffraction results for annealed gold and silver films on glass.

**Table 1.** Film Thickness, Contact Angles for Water, Glycerol, and Diiodomethane, and Surface Energies and Their Polar and Dispersive Components for SAMs on Gold

	-CH <sub>3</sub>	-CF <sub>3</sub>	-OH	-F	-Cl	-Br	-I	-H	-CO <sub>2</sub> Et	-CHOHCH <sub>3</sub>
thickness (Å)	13	13	13	12	13	14	15	14	15	14
H <sub>2</sub> O <sub>Adv</sub> (deg)	85	85	30	84	90	81	79	73	65	60
H <sub>2</sub> O <sub>Red</sub> (deg)	81	81	28	79	85	77	75	69	64	56
glycerol <sub>Adv</sub> (deg)	78	78	15	71	72	65	64	62	62	58
CH <sub>2</sub> I <sub>2</sub> <sub>Adv</sub> (deg)	40	59	21	40	37	28	24	13	37	18
γ <sub>s</sub> <sup>exp</sup> (dyn/cm <sup>2</sup> )	40.0	30.9	67.3	40	41.1	45.2	46.8	50.5	46.5	53.5
γ <sub>s</sub> <sup>d</sup> (dyn/cm <sup>2</sup> )	37.5	26.2	37.0	37.4	40.2	42.7	43.9	46.0	35.4	42.2
γ <sub>s</sub> <sup>p</sup> (dyn/cm <sup>2</sup> )	2.5	4.7	30.3	2.6	0.8	2.5	2.9	4.5	11.1	11.3

	-OEtOMe	-NO <sub>2</sub>	-N(CH <sub>3</sub> ) <sub>2</sub>	-SH	-SCH <sub>3</sub>	-COCH <sub>3</sub>	-pyridine
thickness (Å)	16	14	15	13	15	15	13
H <sub>2</sub> O <sub>Adv</sub> (deg)	61	64	66	67	70	55	28
H <sub>2</sub> O <sub>Red</sub> (deg)	58	59	62	62	64	51	25
Glycerol <sub>Adv</sub> (deg)	66	46	50	60	63	58	25
CH <sub>2</sub> I <sub>2</sub> <sub>Red</sub> (deg)	39	20	28	23	24	36	13
γ <sub>s</sub> <sup>exp</sup> (dyn/cm <sup>2</sup> )	47.7	51.6	48.9	49.9	48.7	51.6	69.0
γ <sub>s</sub> <sup>d</sup> (dyn/cm <sup>2</sup> )	33.7	42.3	39.8	41.9	42.1	34.3	38.9
γ <sub>s</sub> <sup>p</sup> (dyn/cm <sup>2</sup> )	14.0	9.3	9.1	8.0	6.6	17.3	30.1

**Table 2.** Advancing and Receding Contact Angles for SAMs on Silver Surfaces

	-CH <sub>3</sub>	-CF <sub>3</sub>	-OH	-F	-Cl	-Br	-I	-H	-CO <sub>2</sub> Et	-CHOHCH <sub>3</sub>
H <sub>2</sub> O <sub>Adv</sub> (deg)	85	95	30	85	90	83	80	71	67	57
H <sub>2</sub> O <sub>Red</sub> (deg)	81	90	28	79	84	78	74	66	63	52

	-OEtOMe	-NO <sub>2</sub>	-N(CH <sub>3</sub> ) <sub>2</sub>	-SH	-SCH <sub>3</sub>	-COCH <sub>3</sub>	-pyridine
H <sub>2</sub> O <sub>Adv</sub> (deg)	64	64	63	71	77	53	29
H <sub>2</sub> O <sub>Red</sub> (deg)	59	59	58	67	72	48	26

AFM studies of surface topography for annealed gold and silver films on glass show 4000–5000 Å and several micrometer grains for the gold and silver surfaces, respectively. X-ray results (Figure 4) show that the gold film surface has a (111) structure, while the silver film surface contains less than 0.1% (100) structure. No difference could be detected between gold and silver substrates prepared using glass slides and their counterparts prepared using silicon wafers.<sup>42</sup>

SAMs were assembled from ethanol solutions, usually of 10 μM concentration, under nitrogen, overnight. The substrates were removed from solution, rinsed with ethanol, and blown dry by a jet of nitrogen. Monolayers could be stored in pure ethanol, at room temperature, for

a later analysis. The thickness of the SAMs was estimated using ellipsometry, and the wetting behavior was examined using different liquids. These measurements were carried out immediately after monolayer formation. We have observed a tendency of forming multilayers from more concentrated solutions. In some cases even when gold substrates were used, e.g., for X = SH and for the pyridine derivative (XVII in Figure 1), concentrations of 0.5 μM had to be employed to ensure only monolayer formation.

The effect of surface roughness of gold on the quality of the resulting SAMs has been demonstrated by the difference between the water advancing and receding contact angles (contact angle hysteresis,  $\Delta\theta = \theta_a - \theta_r$ ). When SAMs were formed on gold surfaces of substrates prepared by the traditional procedure, i.e., room-temperature evaporation of gold on a chromium or titanium adhesion layer, water contact angle hysteresis was ~20°. However, SAMs on the annealed gold show a much smaller hysteresis  $\leq 6^\circ$  (Figure 5). This is in agreement with the reduced surface roughness of the annealed substrates.

(42) Heating of substrates in vacuum prior to gold evaporation has been reported by a number of groups. See: (a) Stevenson, K. J.; Gao, X. P.; Hatchett, W.; White, H. S. *J. Electroanal. Chem.* **1998**, *447*, 43. (b) Dishner, M. H.; Ivey, M. M.; Gorer, S.; Hemminger, J. C.; Feher, F. *J. Vac. Sci. Technol.* **1998**, *16*, 3295. (c) Levlin, M.; Laakso, A.; Niemi, H. E. M.; Hautajarvi, P. *Appl. Surf. Sci.* **1997**, *115*, 31. Microscope slides as substrates for Au evaporation have been used before by the Rubinstein group.

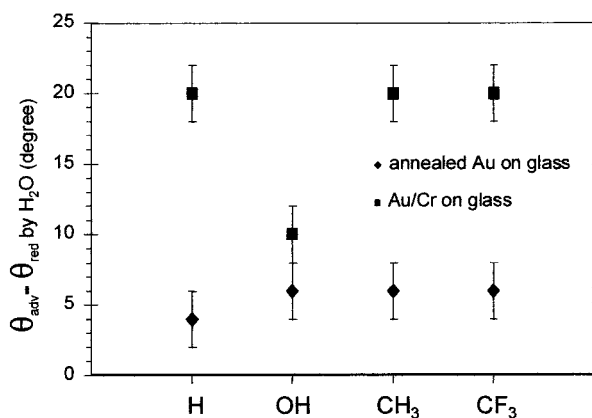


**Figure 5.** Water contact angle hysteresis on SAMs on annealed gold and on Au/Cr on glass.

The measurements of the thickness, contact angle, and calculated surface energy are listed in Tables 1 and 2. The thickness ranges from 12 to 16 Å, suggesting that the molecules are oriented with a small tilt angle with respect to the surface normal. This is in agreement with FTIR data, as will be discussed later. Since hexadecane wets all SAM surfaces, we have measured the contact angles of water, glycerol, and diiodomethane ( $\gamma_{lv} = 72$ , 63, and 50 dyn/cm<sup>2</sup>, respectively). Contact angles are smaller than for the corresponding alkanethiolate SAMs, in agreement with the polar nature of the biphenyl adsorbates.

For example, the advancing water contact angle for a close-packed SAM of octadecanethiolate on gold is 112°, while for the 4'-methyl-4-mercaprobiphenyl SAM it is only 85°. Also, while for alkanethiolate SAMs termination with trifluoromethyl group increases water contact angle, for SAMs of 4'-methyl-4-mercaprobiphenyl and 4'-trifluoromethyl-4-mercaprobiphenyl water contact angles are identical, due to the increased polarity of the latter as a result of a molecular dipole. Interestingly, water contact angles for SAMs on silver are the same, within experimental error, with the exception of the -CF<sub>3</sub> and -SH substituents, where the water contact angle is higher for SAMs on gold, and the -SCH<sub>3</sub> substituent, where the water contact angle is higher for SAMs on silver. Miller and Abbott reported that contact angles of liquids supported on SAMs formed from alkanethiols on metallic substrates are measurably influenced by van der Waals forces that act between the liquids and metallic substrates (through the SAMs).<sup>43</sup> The data presented here do not show a systematic difference between the two metallic substrates.

To further analyze the SAM surfaces we have used the geometric-mean method<sup>44</sup> to calculate their total surface free energy ( $\gamma_s^{exp}$ ), as well as the dispersive ( $\gamma_s^d$ ) and polar ( $\gamma_s^p$ ) components from the advancing contact angles of diiodomethane and water. The values are presented in Table 1.

Fourier transform infrared spectra (FTIR) of all 4'-substituted-4-mercaprobiphenyls and their SAMs were studied in transmission mode for a KBr pellet of the solid and in the external reflection (ER) mode for the SAMs on gold and silver, respectively. Figure 6 presents the ER-FTIR spectra of 4'-trifluoromethyl-4-mercaprobiphenyl in KBr, in CCl<sub>4</sub> solution (5 mM), and in a SAM on gold. The simplification of the spectrum in the SAM environment

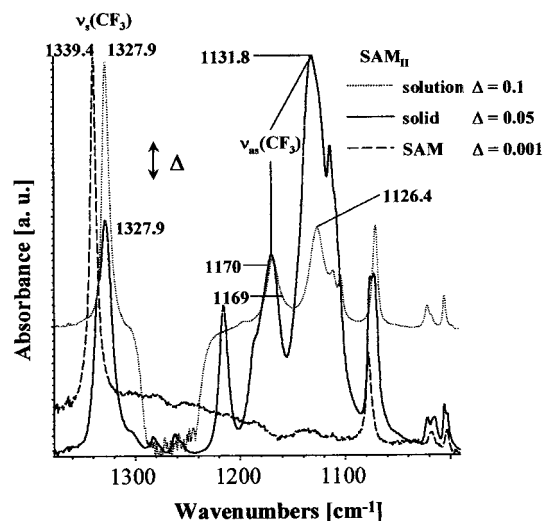


**Figure 6.** The ER-FTIR spectra of 4'-trifluoromethyl-4-mercaprobiphenyl in KBr, in CCl<sub>4</sub> solution (5 mM), and in a SAM on gold prepared in ethanol.

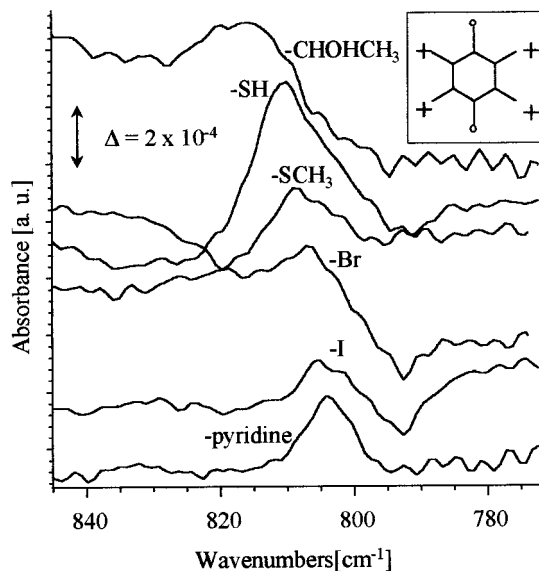


**Figure 7.** Out-of-plane CH wagging B<sub>2</sub> modes around 817 cm<sup>-1</sup> for some SAMs on gold. The insert shows the molecular motion.

reflects the perpendicular orientation of the biphenyl moiety. This suggests that the surface-S-C angle cannot be tetrahedral, but rather close to 180°, which is in agreement with theoretical calculations.<sup>38</sup> There, it was suggested that depending on molecular interactions the hybridization of the S atom might be either sp or sp<sup>3</sup>.

In transmission IR of the solid, the band at 817 cm<sup>-1</sup> is assigned to out of plane CH wagging mode (B<sub>2</sub>). In the ER-FTIR spectra of SAMs on gold and silver, however, the bands around 817 cm<sup>-1</sup> have intensities much weaker than those in the solid state. The bands around 817 cm<sup>-1</sup> for selected SAMs are presented in Figure 7. The dramatic diminution of the band intensity in the SAMs is a result of the small molecular tilts, since this wagging vibration is directed perpendicular to the biphenyl plane.

The medium band around 1000 cm<sup>-1</sup> is assigned as B<sub>1u</sub> & A<sub>1</sub> mode, which is one of the semicircle modes in the region 1150–1003 cm<sup>-1</sup> (Figure 8). The sensitivity of band position and absorption area to the dipole moment of the molecule is evident.<sup>45</sup> It is suggested that this aromatic vibration incorporates a C-T stretching, where T is the atom of 4'-substituent directly attached to 4' position of

(43) Miller, W. J.; Abbott, N. L. *Langmuir* **1997**, *13*, 7106.

(44) Wu, S. *Polymer Interface and Adhesion*; Marcel Dekker: New York, 1982.

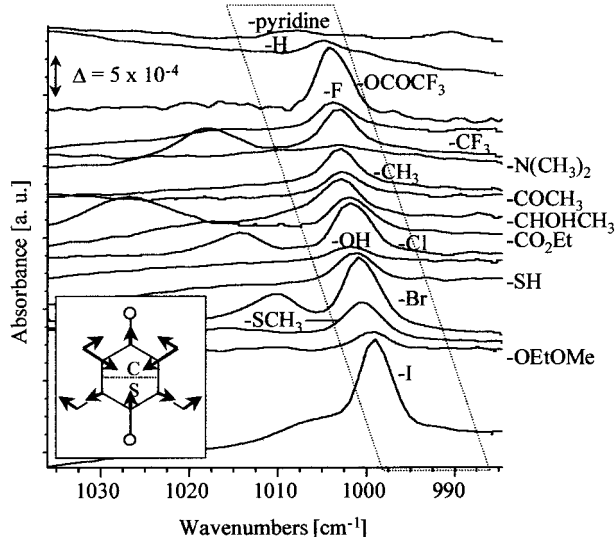


**Figure 8.** The  $B_{1u}$  &  $A_1$  semicircle stretch around  $1000\text{ cm}^{-1}$  for SAMs on gold. The insert shows the molecular motion.

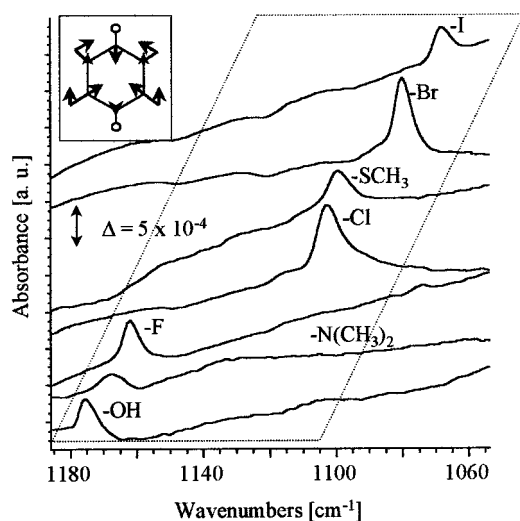


**Figure 9.** The  $B_{1u}$  &  $A_1$  ring C–C vibration and in-plane C–H bending in the  $1180\text{--}1060\text{ cm}^{-1}$  region for SAMs on gold. The insert shows the molecular motion.

the mercaptobiphenyl. The absorption bands around  $1000\text{ cm}^{-1}$  are displayed in Figure 8 for 17 mercaptobiphenyl SAMs on gold, including trifluoroacetyl group, in the order of their band positions.

The nature of the 4'-substituent affects both the position and the integrated area (or intensity) of the bands. It is noticeable that the position and integrated area of the bands for 4'- $\text{CF}_3$ ,  $\text{CH}_3$ ,  $\text{CO}_2\text{Et}$ ,  $\text{CHOHCH}_3$ , and  $\text{C}(\text{O})\text{CH}_3$ , are the same, since in all cases a carbon atom is directly connected to the 4'-position, and hence it is a C–C stretching that participates. The C–T bond strength, affected by T, also plays a role. In the case where X = halogen, the band of the 4'-F has the highest energy and lowest intensity due to its highest electronegativity and lowest atomic weight.

One of the most C–T-sensitive aryl bands is in the region  $1060\text{--}1180\text{ cm}^{-1}$  (Figure 9). This sensitivity results from the fact that during vibration, the C–T bond length increases when the distance between ring carbons 1 and 4 decreases. The resulting direction of dipole moment change is parallel to the 1,4 axis of the ring. In Figure 9,

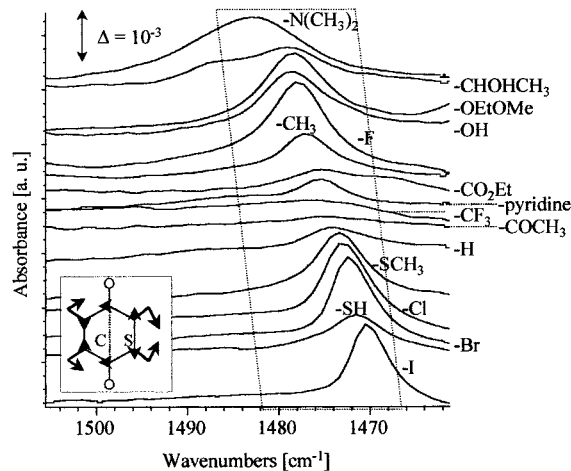


**Figure 10.** The  $E_{1u}$  &  $B_1$  semicircle stretch bands around  $1470\text{ cm}^{-1}$  for SAMs on gold. The insert shows the molecular motion.

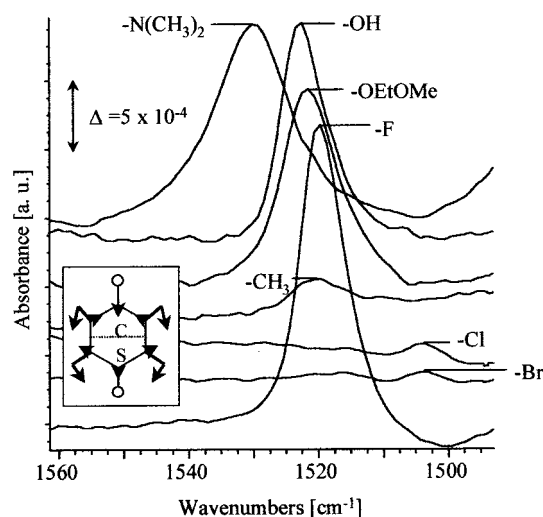


**Figure 11.** The semicircle stretch  $E_{1u}$  &  $A_1$  around  $1520\text{ cm}^{-1}$  for SAMs on gold. The insert shows the molecular motion.

the aryl bands at  $1174$ ,  $1169$ , and  $1162\text{ cm}^{-1}$  correspond to T = O, N, and F, respectively, and are the highest energy bands in the series. The second series of bands is located at  $1103$  and  $1099\text{ cm}^{-1}$  when T is Cl and S; the third series is located at  $1080$  and  $1068\text{ cm}^{-1}$  when T is Br and I. This follows the order of size and electronic properties of these elements.

There are two-semicircle stretching and two quadrant-stretching bands in region  $1400\text{--}1600\text{ cm}^{-1}$ . The band around  $1470\text{ cm}^{-1}$  (Figure 10) is assigned as  $E_{1u}$  &  $B_1$  mode. Except for  $\text{CF}_3$ ,  $\text{CO}_2\text{Et}$ , and  $\text{C}(\text{O})\text{CH}_3$  SAMs, that exhibit very weak absorption due to their electron attracting nature, all other SAMs show significant absorption bands at different wavenumbers, which are distributed in a slightly larger span than the bands around  $1000\text{ cm}^{-1}$ . The order of the bands around  $1470\text{ cm}^{-1}$  follows more or less the order of T as described above. The bands of high wavenumbers are associated with T = N, O, and F, and those of low wavenumbers are associated with T = S, Cl, Br, and I.

The bands around  $1520\text{ cm}^{-1}$  (Figure 11) are assigned as  $E_{1u}$  &  $A_1$  modes. Only SAMs with 4'-substituents of  $\text{N}(\text{CH}_3)_2$ , OH,  $\text{OCH}_2\text{CH}_2\text{OMe}$ , F,  $\text{CH}_3$ , Cl, and Br show this absorption. Figure 12 presents the bands around  $1600\text{ cm}^{-1}$  that are assigned as  $E_{2g}$  &  $A_g$  mode. In this case, band distribution is even larger ( $1618\text{--}1585\text{ cm}^{-1}$ ) than for bands around  $1470$  and around  $1600\text{ cm}^{-1}$ . This is

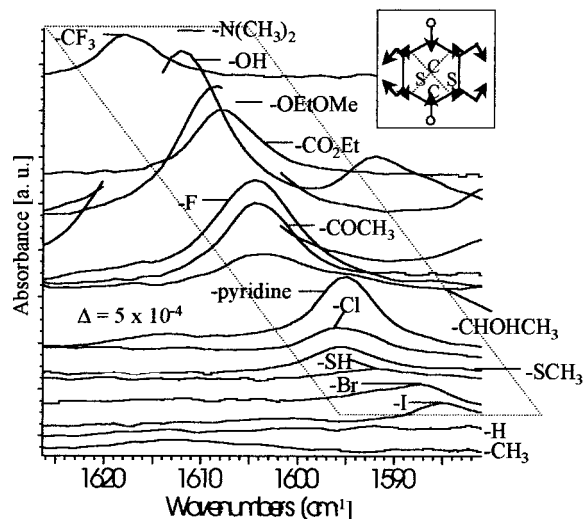


**Figure 12.** The  $E_{2g}$  &  $A_g$  quadrant stretch around  $1600\text{ cm}^{-1}$  for SAMs on gold. The insert shows the molecular motion.

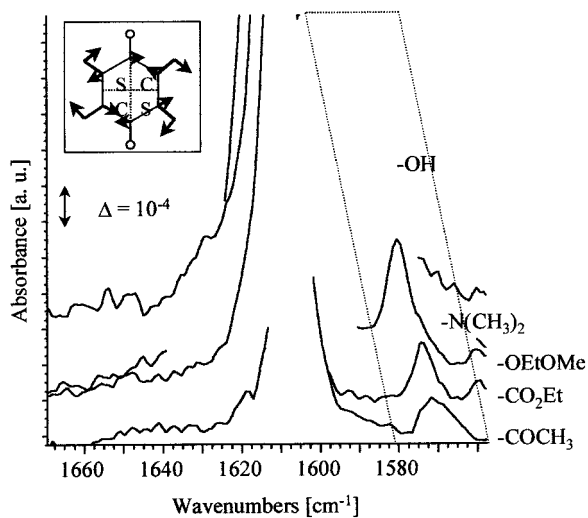


**Figure 13.** The  $E_{2g}$  &  $B_1$  quadrant stretch around  $1580\text{ cm}^{-1}$  for SAMs on gold. The insert shows the molecular motion.

attributed to another important ring skeletal mode, where the transition dipole moment of biphenyl corresponding to T is not only intense but also directed parallel to 1,4-molecular axis. Either electron-donating groups ( $N(\text{CH}_3)_2$ , OH, and  $\text{OCH}_2\text{CH}_2\text{OME}$ ) or electron-attracting groups ( $\text{C}(\text{O})\text{CH}_3$  and  $\text{CO}_2\text{Et}$ ) result in strong IR bands. This is due to the significant increase in molecular dipole, which is parallel to the 1,4-positions of rings. In comparison, the bands for SH,  $\text{CH}_3$ , and parent 4-mercaptobiphenyl are barely detected.

The 4-(4-mercaptophenyl)pyridine behaves like 4'-substituted-4-mercapto-biphenyl. In general, changes in electron density distribution that result from a substituent not only shift the band to higher energy but also generate stronger IR absorption. The unexpectedly large shift of 4'- $\text{CF}_3$ , when T is C, could be due to the electronegativity of the fluorine atoms.

Figure 13 shows the bands around  $1580\text{ cm}^{-1}$  that are assigned as the  $E_{2g}$  &  $B_1$  mode. These are much weaker than the bands around  $1600\text{ cm}^{-1}$  and are visible only when the latter are very strong. The effect of the 4'-substituents on band position is observed. As before, strong electron-donating and -attracting groups (OH,  $N(\text{CH}_3)_2$ ,  $\text{OCH}_2\text{CH}_2\text{OCH}_3$ ,  $\text{CO}_2\text{Et}$ ,  $\text{C}(\text{O})\text{CH}_3$ , and F) result in stronger absorption bands.

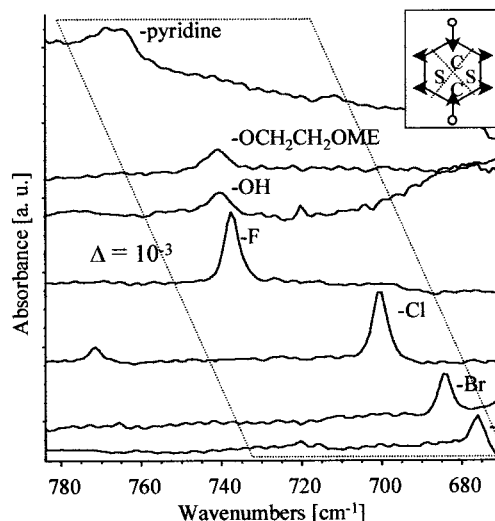


**Figure 14.** The quadrant in-plane bending  $E_{2g}$  & CH stretch around  $740\text{ cm}^{-1}$  for SAMs on silver. The insert shows the molecular motion.

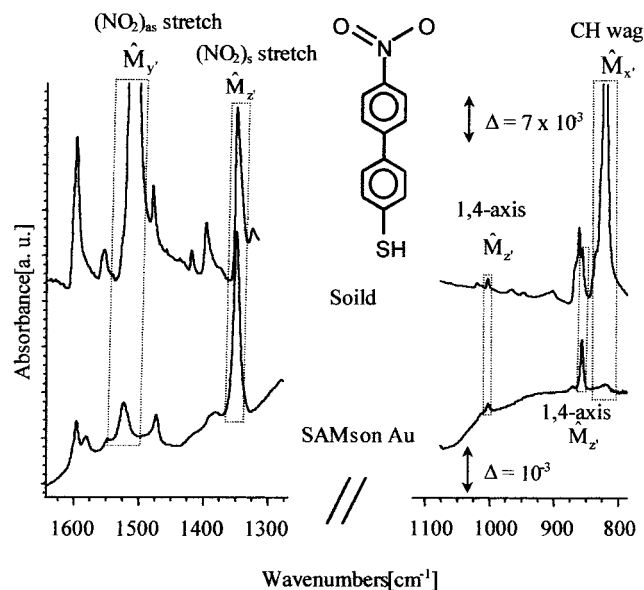


**Figure 15.** The  $\nu_s(\text{NO}_2)$  and  $\nu_{as}(\text{NO}_2)$  bands in the ER-FTIR spectrum of the SAM and transmission spectrum of the solid.

The quadrant bending bands ( $E_{2g}$  & CH stretch) around  $700\text{ cm}^{-1}$  are shown in Figure 14 for SAMs on silver. We have noticed no significant differences in ER-FTIR spectra between the SAMs on gold and on silver, with the exception of minute changes in intensity and band positions. In general, the discussion above can be applied to SAMs on silver. For example, the effect of T on the band position is similar to that discussed above for SAMs on gold as shown in Figure 14.

We now turn to cases where molecular orientation could be calculated from ER-FTIR spectra. In Figure 15 the vibration modes in the ER-FTIR of the SAMs, and in the transmission IR of solid, for the  $\text{NO}_2$  derivative are compared. The intensities of the wagging and the  $\nu_{as}(\text{NO}_2)$  bands are significantly stronger in solid than in SAMs while the  $\nu_s(\text{NO}_2)$  stretching bands in both spectra are comparable.

Figures 16 and 17 show the corresponding comparisons for the cases of  $\text{C}(\text{O})\text{CH}_3$  and  $\text{CO}_2\text{Et}$ . In Figure 16, the  $\nu_{as}(\text{CH}_3)$  band is significantly weaker in SAMs than in the solid, while the  $\nu_s(\text{CH}_3)$  bands in both spectra are

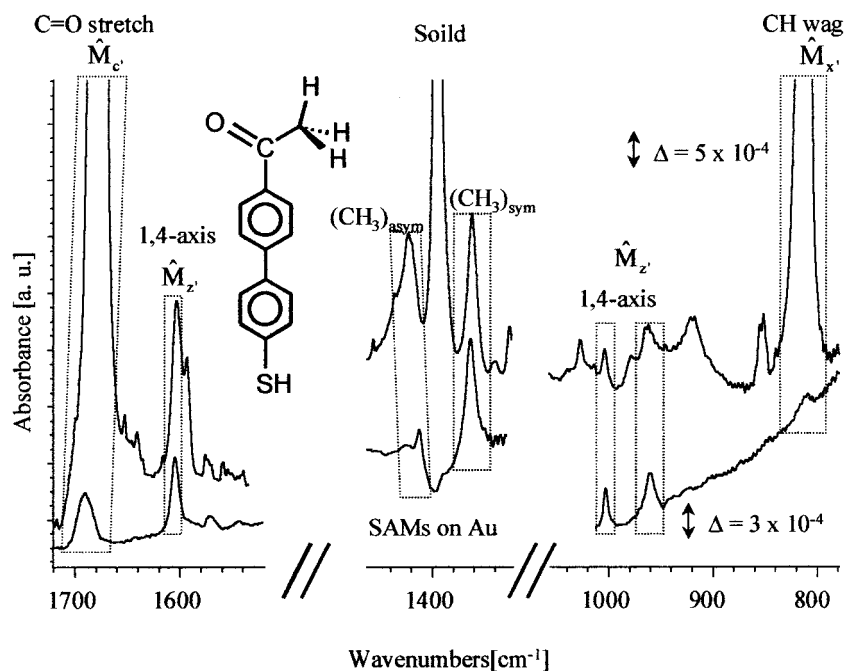


**Figure 16.** The C=O stretching,  $\nu_s(\text{CH}_3)$ ,  $\nu_{as}(\text{CH}_3)$ , and wagging bands in the ER-FTIR spectrum of the SAM and transmission spectrum of the solid.

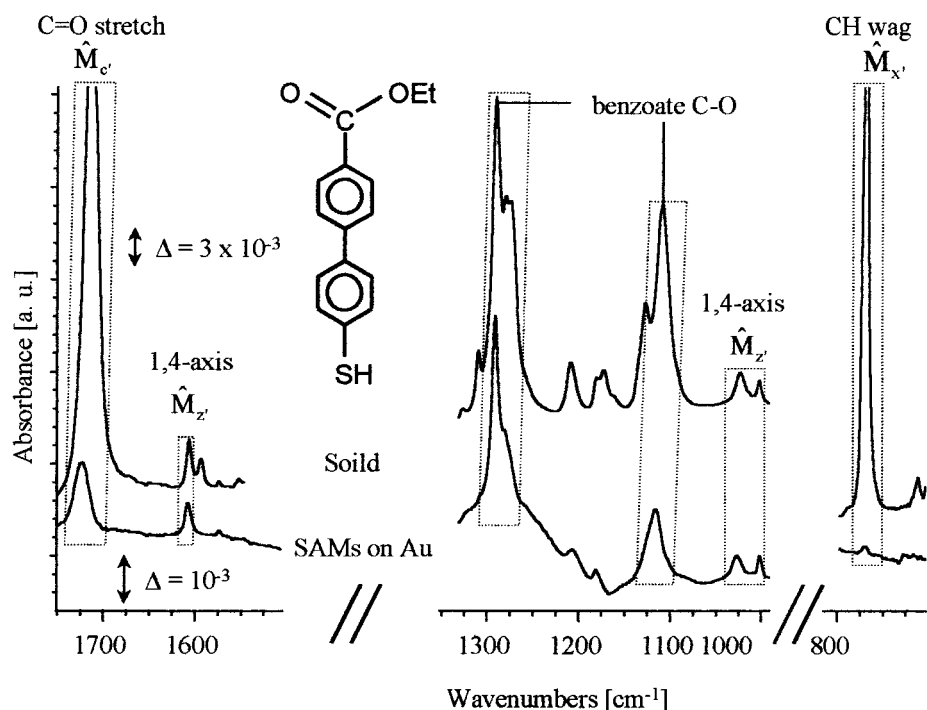


**Figure 17.** The C=O stretching, benzoate C–O stretching, and wagging bands in the ER-FTIR spectrum of the SAM and transmission spectrum of the solid.

comparable. Similarly, in Figure 17, the absorbance of the benzoate C–O stretching band is about half that for the transmission band, while the bands of the 1,4-axis ring modes in both spectra are comparable. All these observations are in agreement with our estimation using Euler's angles, as will be discussed below.

The ER-FTIR spectra of SAMs on silver are similar to that on gold. The calculated tilt angles of biphenyl plane away from the surface normal and rotation around 1,4 axis are not different from that on gold. With the same molecular orientation, the slightly larger wavenumber and absorbance of SAMs on silver demonstrate the

possibility that the molecules in the SAMs on silver may be more closely packed than those on gold. Figure 18 presents one representative comparison among spectra of the  $\text{N}(\text{CH}_3)_2$  derivative in the solid state and in SAMs on gold and silver. The blue- and red-shifts around 1600 and 1470  $\text{cm}^{-1}$ , respectively, of the bands for SAMs on gold and silver as compared to the solid materials hint that differences in the packing structures exist between the SAMs and the solid.

To calculate molecular orientation, we have made three assumptions. First, that the average orientation of organic molecules in a solid is isotropic. Second, that the vibra-

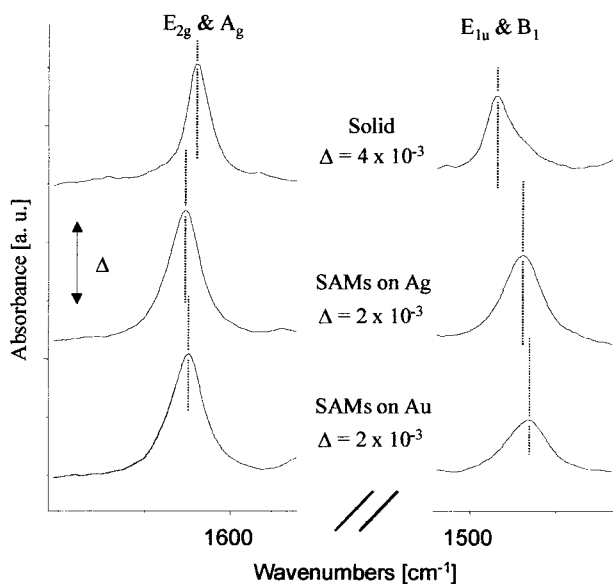


**Figure 18.** A comparison between transmission and ER-FTIR for the  $E_{2g}$  &  $A_g$  and  $E_{1u}$  &  $B_1$  bands for the  $(\text{CH}_3)_2\text{N}$ - derivative.

tional oscillator strengths probably change when the mercaptobiphenyl is bonded to the surface but that these changes are not very different for all derivatives studied. Third, that the ratio of the band absorbance of the molecule in its SAM to that of the molecule in the solid state may provide an estimate for the projection of the specific transition with respect to the surface normal. Notice that the SAMs are not uniaxial with respect to the  $Z$ -axis.

The 4'-mercaptobiphenyl moieties are effectively completely planar,<sup>46</sup> and hence the only degrees of freedom are tilt and rotation about the molecular axis. If the molecules were perpendicular to the surface, there was no meaning to rotation about molecular axis, since all vibrations that are perpendicular to the plane of the benzene rings are parallel to the SAM surface and hence are not visible in a grazing angle FTIR spectrum. The same is true for planar substituents such as nitro ( $\text{NO}_2$ ) acetyl  $\text{C}(\text{O})\text{CH}_3$ , and ethoxycarbonyl ( $\text{CO}_2\text{Et}$ ), assuming that they are coplanar with the benzene ring due to strong conjugation. Once the molecules in the SAM are tilted with respect to the surface normal, the rotation about the molecular axis becomes meaningful, since it defines the projection of a vibration that is perpendicular to the benzene ring on the  $Z$ -axis and, hence, the absorbance. Infrared spectra show that the molecules in the SAMs are tilted; hence Euler's angles<sup>47</sup> (Figure 19) are a useful mathematical tool for the calculation of surface molecular orientation.

In these calculations, one Cartesian coordinate system is fixed, where  $X$  and  $Y$  are assigned to the metal surface plane and  $Z$  is fixed at the surface normal. An additional set of coordinates ( $X'$ ,  $Y'$ ,  $Z'$ ) is assigned to the molecule and is free to move with the biphenyl plane and thus determined the two Eulerian angles,  $\theta$  (tilt) and  $\psi$  (rotation).<sup>48</sup>

In SAMs of  $\text{NO}_2$ ,<sup>49</sup>  $\text{C}(\text{O})\text{CH}_3$ , and  $\text{CO}_2\text{Et}$ , three orthogonal modes can be utilized for the calculations. For example,

(46) von Laue, L.; Ermark, F.; Götzhäuser, A.; Haebleren, U.; Häcker, U. *J. Phys. Condens. Matter* **1996**, *8*, 3977.

(47) Debe, M. K. *Appl. Surf. Sci.* **1982**, *14*, 1.

(48) Corben, H. C.; Stehle, P. *Classical Mechanics*; John Wiley & Sons: New York, 1950; p 174.

(49) Kang, J. F.; Ulman, A.; Liao, S.; Jordan, R. *Langmuir* **1999**, *15*, 2095.

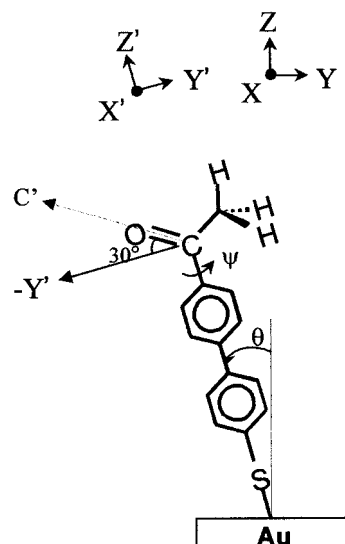


**Figure 19.** Euler's angles for SAMs of 4'-acetyl-4'-mercaptobiphenyl.

the three bands used for the calculation in the case of the 4'- $\text{NO}_2$  derivative are the wagging band around  $700\text{ cm}^{-1}$  ( $X'$ ), the  $\nu_{\text{as}}(\text{NO}_2)$  ( $Y'$ ), and the  $\nu_{\text{s}}(\text{NO}_2)$  ( $Z'$ ). For the two other SAMs, given the  $\text{sp}^2$  hybridization of carbon, the transition dipole of the  $\text{C}=\text{O}$  group is inclined  $30^\circ$  to the direction perpendicular to the biphenyl main axis, in the molecular plane ( $C'$  axis, Figure 19). By using the ratios between the absorbance values in the ER-FTIR spectra of the SAMs and the transmission spectra of solid materials, the average orientation of molecules relative to the substrate could be calculated. The matrix for the transformation from the primed to the unprimed coordinates is

$$\hat{M}_x = |\hat{M}_x| \hat{x}', \quad \hat{M}_z = |\hat{M}_z| \hat{z}', \\ \hat{M}_y = |\hat{M}_y| \hat{y}' \quad (\text{or } \hat{M}_c = |\hat{M}_c| \hat{c}')$$

If  $\hat{M}_x$ ,  $\hat{M}_y$ , and  $\hat{M}_z$  are the transition moments of an orthogonal group in the  $X'$ ,  $Y'$ , and  $Z'$  axes, respectively, then

$$\hat{M}_x \cdot \hat{z} = |\hat{M}_x| \hat{x}' \cdot \hat{z}, \quad \hat{M}_z \cdot \hat{c}' = |\hat{M}_z| \hat{z}' \cdot \hat{z}$$

$$\hat{M}_y \cdot \hat{z} = |\hat{M}_y| \hat{y}' \cdot \hat{z} \quad (\text{or } \hat{M}_c \cdot \hat{z} = |\hat{M}_c| \hat{c}' \cdot \hat{z})$$

where  $\hat{x}'$ ,  $\hat{z}'$ ,  $\hat{y}'$  (or  $\hat{c}'$ ) and are unit vectors in  $X'$ ,  $Z'$ ,  $Y'$  (or  $C'$ ) axes, respectively. The projection of the vectors at the  $X'$  and  $Y'$  direction on the  $Z'$ -axis (or surface normal) is

$$\begin{pmatrix} x \\ y \\ z \end{pmatrix} = \begin{pmatrix} \cos \psi & -\sin \psi & 0 \\ \sin \psi \cos \theta & \cos \psi \cos \theta & -\sin \theta \\ \sin \psi \sin \theta & \cos \psi \sin \theta & \cos \theta \end{pmatrix} \begin{pmatrix} x' \\ y' \\ z' \end{pmatrix}$$

Assuming that the oscillator strengths of vibrations of the adsorbed molecules are the same as those in the isotropic solid materials, the reduced absorbance  $A_i$  of the  $i$ th vibration mode can be defined as  $A_i = A_{i,\text{ERIR}}/A_{i,\text{transmission}}$ . This cancels out the intrinsic dipole strength of the  $i$ th vibration mode and results in two orientation parameters ( $\theta$  and  $\psi$ ) and in a constant  $\bar{K}$ , as shown below. For a molecule adsorbed on a planar surface, the

reduced absorbance of the  $i$ th vibration mode is derived as follows.

$$\therefore A_i = \bar{K} \cdot |\hat{M}_i \cdot \hat{E}|^2 / (|\hat{M}_i|^2 \cdot |\hat{E}_z|^2)$$

$$\therefore A_x = \bar{K} \cdot \sin^2 \psi \sin^2 \theta$$

$$A_z = \bar{K} \cdot \cos^2 \theta$$

$$A_y = \bar{K} \cdot \cos^2 \psi \sin^2 \theta$$

or

$$A_c = \bar{K} \cdot \left[ -\frac{3^{1/2}}{2} \sin \theta \cos \psi + \frac{1}{2} \cos \theta \right]^2$$

$$\Rightarrow \frac{A_x}{A_y} = \tan^2 \psi$$

or

$$\frac{A_x}{A_z} = \sin^2 \psi \tan^2 \theta$$

$$\frac{A_y}{A_z} = \cos^2 \psi \tan^2 \theta$$

$$\frac{A_c}{A_z} = \left[ -\frac{3^{1/2}}{2} \tan \theta \cos \psi + \frac{1}{2} \right]^2$$

The reduced absorbance values for  $A_x$ ,  $A_y$ ,  $A_c$ , and  $A_z$  are directly obtained from the ratios of the absorbance of the band in the ER-FTIR spectrum to that in transmission IR spectrums. The resulting tilt angles ( $\theta$ ) away from the surface normal and the rotation angle ( $\psi$ ) around the 1,4-axis of the biphenyl are listed in Table 3 for SAMs on gold and in Table 4 for SAMs on silver.

The errors associated with the calculations are  $\pm 2^\circ$  (assuming constant oscillator strengths). Unfortunately, the reduced absorbance  $A_y$  (or  $A_c$ ) is not available for the rest of the 4'-substituted-4-mercaptobiphenyls. Nevertheless, the  $A_z/A_x$  ratios in Table 3, which do not deviate largely from those of C(O)CH<sub>3</sub>, CO<sub>2</sub>Et, and NO<sub>2</sub>, hint that the biphenyl molecules adsorbed on gold in an orientation with a relatively small tilt. This is in agreement with synchrotron X-ray studies of SAMs of 4'-methyl-4-mercaptobiphenyl on gold that estimated for the CH<sub>3</sub> derivative a tilt of less than 19° from the surface normal.<sup>50</sup> Given the assumptions we have made, and hence the expected error associated with ER-FTIR-based calculation, the agreement with the X-ray studies is encouraging.<sup>51</sup>

Contrary to the tilt of alkyl chain in SAMs of alkanethiolates on gold, which is driven by the reestablishment of interchain van der Waals attraction, the more perpendicular molecular orientation<sup>29</sup> in SAMs of mercaptobiphenyl derivatives is probably the result of maximizing  $\pi$ - $\pi$  interactions. However, when the molecules possess strong dipole moments, intermolecular interactions result in instability, and thus the tilt angle may strongly depend on the polarity of the solvent from which the SAM was prepared.<sup>29</sup> For example, while Figure 7 presents the simplified ER-FTIR spectrum of a SAM of 4'-trifluoromethyl-4-mercaptobiphenyl on gold prepared from ethanol, when the same SAM is prepared from a much less polar solvent (toluene), the  $\nu_{as}(\text{CF}_3)$  appears, suggesting a considerably larger tilt angle (Figure 20). Given that

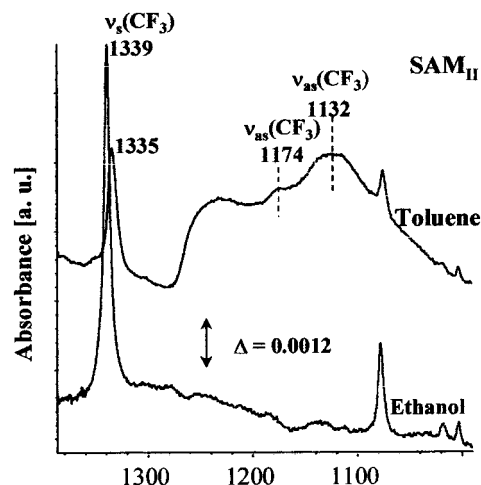


**Figure 20.** The ER-FTIR spectra of 4'-trifluoromethyl-4-mercaptobiphenyl SAM on gold prepared from ethanol and from toluene solutions.

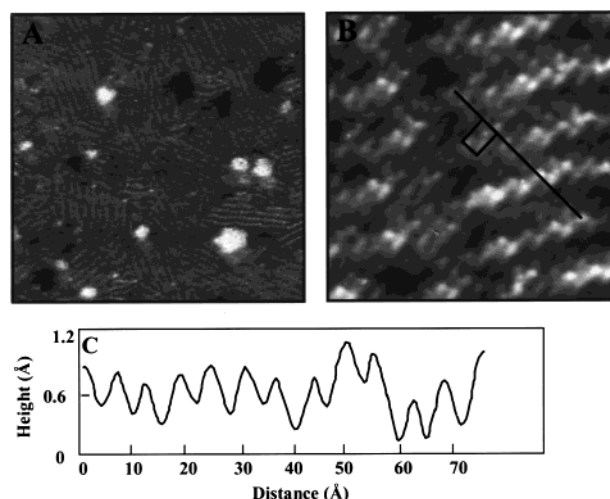


**Figure 21.** (A) An 800 Å × 800 Å constant current STM topography of 4'-chloro-4-mercaptobiphenyls on Au(111) showing different ordered domains. (B) High-resolution STM image (100 Å × 100 Å) of the same sample. The rectangular unit cell is indicated in the image. (C) A cursor profile indicated in Figure 1B. Imaging conditions: 1.2 V and 50 pA.

the tilt angle could be calculated only for three SAMs, it is difficult to suggest a trend, given that other factors, such as the steric requirements of the 4'-substituent and its electronic properties, may play a role.

The conclusion that one draws from these data is that in SAMs of mercaptobiphenyls on gold the molecules have a relatively small tilt from the surface normal. This tilt is the result of a balance between the drive to adsorb more thiols at the surface to gain adsorption energy, which requires the minimum possible cross-sectional area and hence no tilt, and intermolecular repulsion that increases tilt.<sup>28</sup>

It is usually more difficult to achieve high-resolution STM images for 4'-chloro-4-mercaptobiphenyl SAMs than *n*-alkanethiol SAMs on Au(111) due to relatively smaller domains and high density of defects. Figure 21A shows a typical STM image, taken in UHV, of a 4'-chloro-4-mercaptobiphenyl SAM on the Au(111) surface (800 Å × 800 Å). The surface consists of ordered domains with an average size of 50–100 Å. Two important structural features are observed in the STM images. First, six equivalent domains are present (Figure 21) and the orientations of these domains with respect to the three

(50) Leung, T. Y. B.; Kang, J. F.; Scoles, G.; Ulman A. *Surf. Sci.* **2000**, *458*, 34.

(51) One of the referees of this paper has noted that significant band shifts and changes in band shape might lead to errors in estimated angles and suggested that a more general statement that molecular tilt in these SAMs is between 10 and 20° is sufficient.

**Table 3. Values of  $A_z/A_x$  Ratios, the Tilt Angles ( $\theta$ ) Away from the Surface Normal, and the Rotation Angle ( $\psi$ ) around the 1,4-Axis for SAMs on Gold**

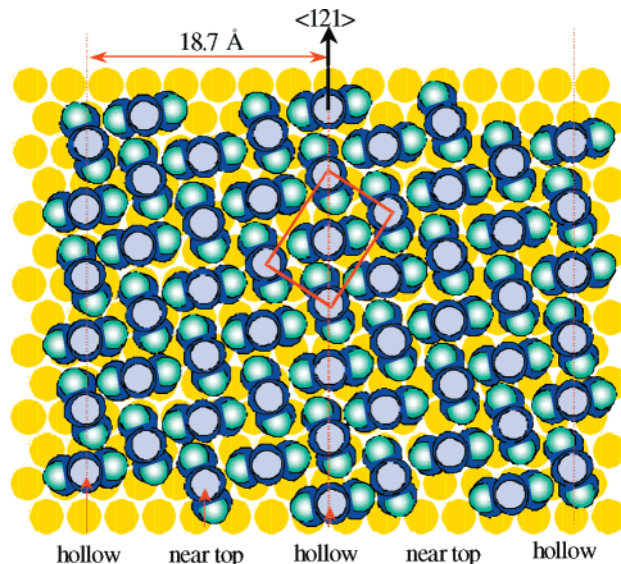
	-F	-Cl	-Br	-I	-CH <sub>3</sub>	-OH	-H	-SH	-SCH <sub>3</sub>
$A_z/A_x$	64	69	133	101	125	74	55	16	63
	-N(CH <sub>3</sub> ) <sub>2</sub>	-CHOHCH <sub>3</sub>	-NO <sub>2</sub>	-COCH <sub>3</sub>	-CO <sub>2</sub> Et	-pyridine	-CH <sub>3</sub>	-OEtOMe	
$A_z/A_x$	79	15	84	105	96	7	118	70	
$\theta$ (deg)			14	20	12				
$\psi$ (deg)			30	15	30				

**Table 4. The Tilt Angles ( $\theta$ ) away from the Surface Normal and the Rotation Angle ( $\psi$ ) around the 1,4-Axis for SAMs on Silver**

	NO <sub>2</sub>	COCH <sub>3</sub>	CO <sub>2</sub> Et
$\theta$ (deg)	8	21	11
$\psi$ (deg)	32	10	31

$\langle 121 \rangle$  directions of Au(111) are  $\pm 5^\circ$ . The observed orientations deviated from the hexagonal symmetry of the Au(111) substrate, which suggests that the lattice of SAMs is not commensurate with respect to the Au(111) lattice. Second, superstructures are observed, as evidenced by the presence of periodical ridges within each ordered domain (Figure 21A). The interstripe spacing is  $18.1 \pm 1.0$  Å. The superstructure is more clearly visible in the higher resolution STM image shown in Figure 21B, in which the molecular periodicity is modulated by the stripe features, e.g., every four molecules along the row have the similar topographic height. The molecular level corrugation is  $0.6 \pm 0.3$  Å. These ridges are oriented along the diagonal direction of the rectangular unit cell. As shown in the cursor profile in Figure 21C, the lattice constants extracted from Figure 21B are  $a = 5.5 \pm 0.3$  Å,  $b = 8.0 \pm 0.5$  Å, and  $\alpha = 90^\circ \pm 5.0^\circ$ . The measured lattices deviate from the well-known commensurate ( $\sqrt{3} \times 2\sqrt{3}$ )-R30° structure proposed for *n*-alkanethiol SAMs, where  $a = 4.99$  and  $b = 8.64$  Å. The presence of superstructure further demonstrates that 4'-chloro-4-mercaptobiphenyl molecules do not form a simple commensurate lattice on Au(111).

The observed periodicity for 4'-chloro-4-mercaptobiphenyl SAM is very similar to the crystalline structure of biphenyl<sup>26,52</sup> and 4-[4'-(phenylethynyl)-phenylethynyl]-benzenethiol SAMs on Au(111).<sup>53</sup> The proposed structural model is shown in Figure 22, in which the phenyl planes along the  $\langle 121 \rangle$  direction are most closely packed and orientated in a herringbone fashion based upon the crystalline structure of biphenyl. The molecular rows of mercaptobiphenyls are oriented  $55^\circ$  instead of  $60^\circ$  from the  $\langle 121 \rangle$  direction. As a result, six instead of three domains are present. This model can also successfully explain the periodicity and other detailed structural features of the superlattice. For instance, the interstripe spacing is 18.7 Å. The corrugation of the superlattice can be explained by various adsorption sites of the sulfur headgroups on the Au(111) surface such as triple-hollow, bridge, and top sites, etc. For every four molecules along the row, sulfur atoms adsorb on the same surface sites such as the triple-hollow site of Au(111). This incommensurate structure of a SAM is the result of the interplay among the headgroup substrate and between biphenyl moiety interactions. The observed SAM structure suggests that the intermolecular interactions among 4'-chloro-4-mercaptobiphenyl molecules are dominant within SAMs, thus not all of the sulfur headgroups adsorb on the triple hollow sites as in the commensurate ( $\sqrt{3} \times 2\sqrt{3}$ )R30°

**Figure 22.** Schematic diagram of the proposed structural model for 4'-chloro-4-mercaptobiphenyl SAMs on Au(111).

structure. We have not yet imaged SAMs on Ag(111) surfaces, but expect similar structure because of the intermolecular interactions. The difference between the X-ray diffraction results<sup>50</sup> and the present STM data is the first demonstration that different substituents at the 4'-position of 4-mercaptobiphenyls (CH<sub>3</sub> and Cl, respectively) results in different packing arrangements in SAMs on gold.

## Conclusions

We have prepared, characterized, and studied SAMs of rigid 4'-substituted-4-mercaptobiphenyls on planar Au(111) and Ag(111) substrates. These monolayers show lower contact angles than their corresponding alkanethiolate SAMs due to the polar nature of the aromatic moieties. Quantitative analysis of infrared spectroscopy, using Eulerian angle, allowed estimation of the average molecular orientation on a surface. In cases where such analysis is possible, it was found that the biphenyl planes are tilted away from the surface normal toward by  $14^\circ$ ,  $20^\circ$ , and  $12^\circ$ , for NO<sub>2</sub>, C(O)CH<sub>3</sub>, and CO<sub>2</sub>Et, respectively, and rotate around the 1,4 axis of the ring at  $30^\circ$ ,  $15^\circ$ , and  $30^\circ$  on gold, respectively. For SAMs on silver, the tilt is  $8^\circ$ ,  $21^\circ$ , and  $11^\circ$ , respectively, and the rotation angles are  $32^\circ$ ,  $10^\circ$ , and  $31^\circ$ , respectively, with errors  $\pm 2^\circ$ . Scanning tunneling microscopy studies indicate that these plate-shaped molecules form incommensurate structures on Au(111) surfaces.

**Acknowledgment.** This work was funded by the NSF through the MRSEC for Polymers at Engineered Interfaces. G.-y.L. thanks the NSF for a Career Award (9733400). R.J. is thankful for the postdoctoral fellowship supported by the Deutsche Forschungsgemeinschaft. We thank Professor G. Scoles of Princeton University for many discussions.

LA001217+

(52) Charbonneau, G.-P.; Delugear, Y. *Acta Crystallogr., Sect. B* **1977**, *33*, 1586.

(53) Yang, G.; Qian, Y.; Engtrakul, C.; Sita, L. R.; Liu, G.-Y. *J. Phys. Chem. B* **2000**, *104*, 9059.